applied sciences

MDPI

Article

Atmospheric Pressure Plasma Irradiation Facilitates Transdermal Permeability of Aniline Blue on Porcine Skin and the Cellular Permeability of Keratinocytes with the Production of Nitric Oxide

Sunmi Lee [1,†], Jongbong Choi [2,†], Junghyun Kim [3], Yongwoo Jang [2,*] and Tae Ho Lim [1,3,*]

[1] Department of Emergency Medicine, Hanyang University Hospital, Seoul 04763, Korea; leesunmi1035@gmail.com
[2] Department of Biomedical Engineering, Hanyang University, Seoul 04763, Korea; cjbonghyu@gmail.com
[3] Research Center, CODESTERI Inc., Seoul 04763, Korea; optimist.jhkim@gmail.com
* Correspondence: ywjang@hanyang.ac.kr (Y.J.); erthim@hanyang.ac.kr (T.H.L.)
† These authors contributed equally to this work.

Abstract: The transdermal delivery system of nutrients, cosmetics, and drugs is particularly attractive for painless, noninvasive delivery and sustainable release. Recently, atmospheric pressure plasma techniques have been of great interest to improve the drug absorption rate in transdermal delivery. Currently, plasma-mediated changes in the lipid composition of the stratum corneum are considered a possible mechanism to increase transdermal permeability. Nevertheless, its molecular and cellular mechanisms in transdermal delivery have been largely confined and still veiled. Herein, we present the effects of cold plasma on transdermal transmission on porcine skin and the cellular permeability of keratinocytes and further demonstrate the production of nitric oxide from keratinocytes. Consequently, argon plasma irradiation for 60 s resulted in 2.5-fold higher transdermal absorption of aniline blue dye on porcine skin compared to the nontreated control. In addition, the plasma-treated keratinocytes showed an increased transmission of high-molecular-weight molecules (70 and 150 kDa) with the production of nitric oxide. Therefore, these findings suggest a promoting effect of low-temperature plasma on transdermal absorption, even for high-molecular-weight molecules. Moreover, plasma-induced nitric oxide from keratinocytes is likely to regulate transdermal permeability in the epidermal layer.

Keywords: atmospheric pressure plasma; transdermal permeability; transdermal delivery; nitric oxide; plasma medicine

Citation: Lee, S.; Choi, J.; Kim, J.; Jang, Y.; Lim, T.H. Atmospheric Pressure Plasma Irradiation Facilitates Transdermal Permeability of Aniline Blue on Porcine Skin and the Cellular Permeability of Keratinocytes with the Production of Nitric Oxide. *Appl. Sci.* **2021**, *11*, 2390. https://doi.org/10.3390/app11052390

Academic Editors: Matteo Zuin and Andrei Vasile Nastuta

Received: 13 January 2021
Accepted: 4 March 2021
Published: 8 March 2021

1. Introduction

The percutaneous transmission of nutrients, cosmetics, and drugs is a painless and noninvasive delivery method wherein they are absorbed by crossing through the skin layers to the systemic circulation [1,2]. In particular, transdermal drug delivery systems using various types of skin patches [3,4] and other transdermal methods, such as ion penetration [5,6] and ultrasound [7,8], have improved absorption rates for local and/or systemic delivery of therapeutic agents through the skin layers. In addition, the atmospheric pressure plasma technique is also of great interest to improve the drug absorption rate in transdermal delivery [9].

In the past couple of decades, cold atmospheric pressure plasma opened up a new frontier in medicine and healthcare as a term of plasma medicine [10–13]. Remarkably, numerous studies have demonstrated biomedical applications for alleviating dermatological problems, such as skin wounds and infections, that are relatively easy to process with plasma [14–17]. In addition, some studies have focused on the effects of cold plasma on the skin barrier, not as a disease treatment but as a drug-delivery technology. For

instance, it was found that atmospheric plasma jet irradiation for 3 min promotes transdermal delivery of hydrophilic rhodamine B dye on rat skin due to a reversible small pore induced by the collision of charged particles [18]. Moreover, further investigations showed a practical transdermal delivery of galantamine hydrobromide (368 Da) and lidocaine (234 Da) used for Alzheimer's disease treatment and local anesthetic, respectively [19,20]. Interestingly, plasma irradiation through atmospheric-pressure plasma jets or dielectric barrier discharge exhibited an increased transdermal delivery of high-molecular-weight lipophilic cyclosporine A (1203 Da), whereas there was no absorption without plasma treatment [21]. Despite evident findings of improved transdermal delivery by plasma, its molecular and cellular mechanism(s) are still elusive.

The stratum corneum is the outermost layer of the epidermis, which is an important component of the skin barrier [22,23]. As the stratum corneum primarily prevents the transdermal absorption of drugs, several studies have suggested increased permeability due to changes in lipid composition in the plasma-treated stratum corneum layer [18,24]. In addition, one remarkable study most recently showed transcriptomic changes in cell junction proteins, cytoskeletal proteins, and extracellular matrix proteins in the stratum corneum of plasma-treated skin [25]. However, it is still unclear how these transcriptomic changes can be induced in the epidermis layer.

The stratum corneum layer is composed of keratinized and flattened corneocytes that are differentiated dead keratinocytes. In the lower stratum corneum, living keratinocytes are connected through cell–cell junctions in the epidermal layer called the stratum granulosum. In the present study, we attempted to investigate the transdermal permeability of our plasma device on porcine skin and further determined the effect of drug delivery and the production of nitric oxide in cultured keratinocytes, which is an important regulator of skin barrier function and includes junctional proteins, cytoskeletal proteins, and extracellular matrix proteins.

2. Material and Method

2.1. Plasma Device

For the present study, we installed an atmospheric-pressure plasma jet device. The outer and inner diameters of the nozzle tube of the device were 3 mm and 2 mm, respectively (Figure 1A). As shown in Figure 1B, dielectric barrier discharge (DBD) jet consists of a high voltage applied hollow electrode, an alumina dielectric with 0.5 mm thickness, and an external ground electrode with a width of 5 mm. Flow control units (RK1600R, Kofloc, Japan) were independently connected to control argon and helium gas, and the flow rate was maintained at 2 standard liters per minute (slm). The DC input source inverted to AC power by push-pull type inverter. The applied AC voltage and discharge current were measured using an oscilloscope (MDO3000, Tektronix, Beaverton, OR, USA), a high voltage probe (P6015A, Tektronix, USA), and a current probe (P6022, Tektronix, USA) to compare the electrical properties of argon and helium plasma jets. The emission spectra of argon and helium plasma jets were measured by varying the wavelength range from 200 to 900 nm through an OES spectral analyzer (HR4000CG, Ocean Optics, Orlando, FL, USA). The optic fiber was connected to the OES spectral analyzer and fixed at a distance of 5 mm from the plasma device nozzle.

2.2. Materials

Aniline blue cream was prepared from cetaphil, glycerin, petrolatum, dicaprylyl ether, dimethicone, glyceryl stearate, cetyl alcohol, seed oil, PEG-30 stearate, tocopheryl acetate, dimethiconol, acrylates/C10-30 alkyl acrylate crosspolymer, benzyl alcohol, phenoxyerhanol, prunus amygdalus duicis oil, prophylene glycol, disodium EDTA, carnomer, sodium hydroxide, aniline blue (1 mg/mL), and purified water to create a cream with an aniline blue concentration of 737.73 μg/g.

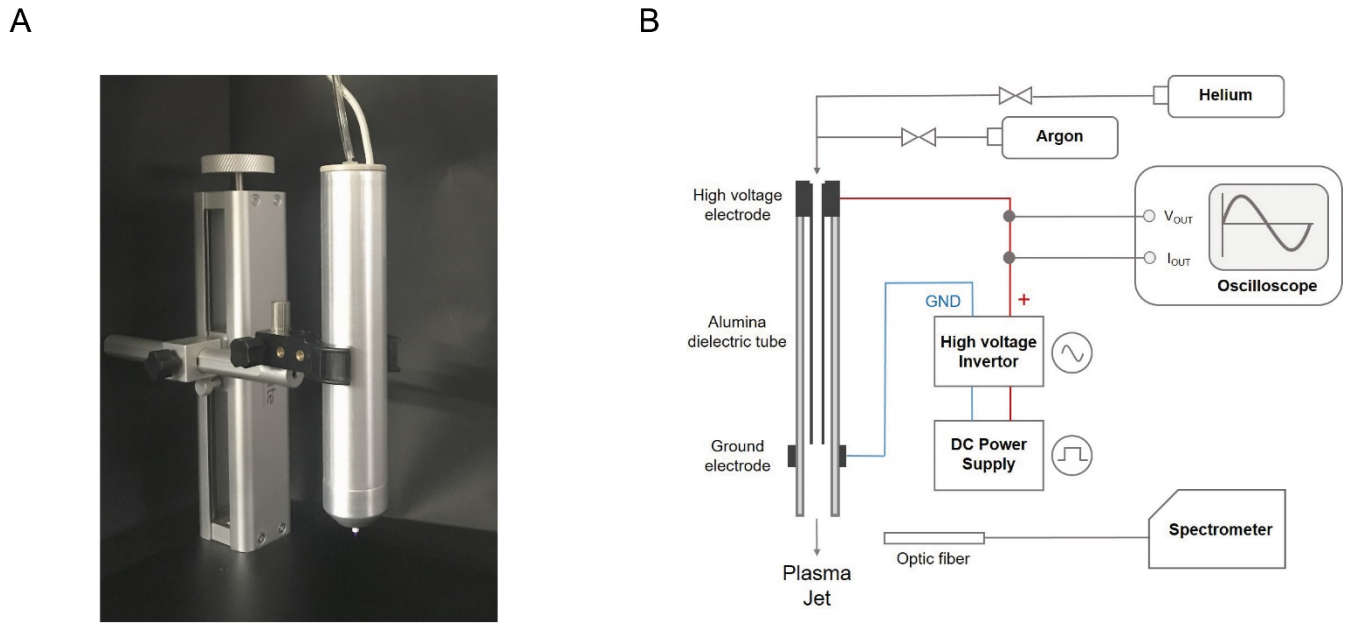

Figure 1. Schematic diagram of the atmospheric pressure plasma jet device. (**A**) Atmospheric pressure plasma jet device used in the present study. (**B**) Schematic diagram of an argon and helium plasma treatment system.

2.3. Permeability of Porcine Skin

Porcine skins were prepared in a size of 2.5 × 2.0 cm. They were divided into four regions of 0.7 × 0.7 cm: no plasma treatment and high-intensity plasma treatment for 10, 30, and 60 s. After the plasma treatment, 1 g of aniline blue cream was applied to the quartered area of porcine skin, and the reaming cream was washed with running water after 5 min. Finally, the aniline blue remaining on the porcine skin after 10 h was quantified by the ImageJ program. The captured picture was executed in the imageJ program. It converted the completed the picture into 8 bit type. To designate the part to be quantified, we used rectangular selection tool of the imageJ program. The rectangular size remained constant for all measurements at each set. The measured values in each set were compared by dividing them into the values of the untreated site (0 s). Finally, statistical analysis was compared based on the experimental results of a total of three sets. Additionally, temperature of porcine skin surface measured using thermal imager (DT 9885, CEM, Shenzhen, China), IR resolution is 384 × 288 pixels and temperature range is from 20 °C to 150 °C. IR image acquisition that we measured in the experiment is 1 spot temperature mode with no zoom.

2.4. Cell Culture

HaCaT cells were cultured in Dulbecco's modified Eagle's medium (DMEM) supplemented with 10% fetal bovine serum (FBS) at 37 °C and 5% CO_2 under previously reported conditions [26].

2.5. Dextran Fluorescein

HaCaT cells (2×10^5) were cultured for 24 h and treated with our plasma device for 30 s in phenol red-free DMEM with 10% FBS. After washing with phosphate-buffered saline (PBS), the cells were further incubated with DMEM containing fluorescein-dextran of 70 or 150 kDa at 37 °C for 1 h. Consequently, the fluorescent dextran in the cells was observed by fluorescence microscopy.

2.6. Measurement of Intracellular Nitric Oxide Level

Intracellular nitric oxide generation was assessed using a QuantiChromTM nitric oxide assay kit (Bioassay Systems, USA). HaCaT cells (2×10^5) were plated on 35-mm

dishes and cultured for 24 h. The cells were deprived of serum for 1 h and treated with our plasma device at multiple time points in phenol red-free medium. After plasma irradiation, cell samples were homogenized in PBS. After centrifugation at 12,000 rpm at 4 °C, the supernatant was used for the nitric oxide assay, and the quantitative colorimetric changes were determined at 540 nm.

2.7. Statistical Analysis

Data analysis was performed with Student's *t*-test for comparisons between two groups or ANOVA with Tukey's hoc test for multiple groups (SPSS 12.0 K for Windows, SPSS, Chicago, IL, USA) to determine the statistical significance (*p* value). Statistical significance was considered for *p* values of <0.05 (*), <0.01 (**), or 0.001 (***).

3. Results and Discussion

3.1. Electrical Properties and Emission Spectra of Argon and Helium Plasma

To analyze the electrical properties, we first measured DC input voltage and DC discharged current, the breakdown voltage of argon and helium gas were 6 V and 4 V, respectively, and discharge currents as breakdown voltage were 0.29 A and 0.25 A at a 2 slm flow rate, respectively (Figure 2A). The DC input voltage conditions for transdermal permeability experiment that length of plasma plume was the longest without plasma arcing and burn in the porcine skin were 18 V and 12 V in argon and helium gas, respectively. As shown in Figure 2B, we measured two cycle waveforms of the inverted AC applied voltage and discharge current of the argon and helium plasma jet at DC input voltage 18 V and 12 V, respectively, and their frequency were 47.28 kHz and 46.67 kHz, respectively. The RMS (Root Mean Square) voltages of argon and helium plasma jets were 2.54 kV and 1.73 kV, respectively, and their RMS discharge currents were 11.01 mA and 6.21 mA at a 2 slm flow rate, respectively. Additionally, the calculated AC power of the argon and helium plasma jet were 4.85 W and 1.86 W, respectively, while DC power was 5.22 W and 3 W, respectively. As previously reported, this difference seems to be caused by argon being relatively easy to ionize because the ionization threshold energies of argon and helium are 15.76 eV and 24.59 eV, respectively [27], even with the increased voltage, the generation of radicals is much higher in argon than in helium plasma [28]. We examined various active species that are observed in argon and helium plasma. The emission spectra of argon and helium plasma indicate that OH (309 nm) and N_2 (310 to 370 nm) were observed in both argon and helium plasma, but NO (283 nm) and N_2^+ first negative bands (391 nm) were observed only in helium plasma (Figure 3). As the ionization threshold energy of N_2 is 14.53 eV, N_2 is likely to be ionized by helium plasma with a metastable energy level of 19.82 eV compared to that of argon plasma (11.5 eV) [29].

3.2. Argon and Helium Plasma Jet Irradiation Increases the Transdermal Permeability of Porcine Skin

The plasma-induced transdermal absorption rate was determined on pig skin, which is known to be most similar to human skin [30]. To optimize the most effective absorption rate condition, we first investigated the transdermal permeability according to the exposure duration of the atmospheric-pressure helium or argon plasma. As shown in Figure 4, the helium or argon plasma was irradiated for 0, 10, 30, and 60 s in the quartered regions of the porcine skin at a distance of 4 mm from the skin surface. Subsequently, a dye reagent (aniline blue cream) was equivalently applied to the quartered porcine skin. After 10 h, the transdermal permeability was analyzed by colorimetric changes depending on the absorbed amount of aniline blue dye. As shown in Figure 4B, argon plasma remarkably facilitated the transdermal absorption of aniline blue on porcine skin in an exposure time-dependent manner. This consequently resulted in approximately 2.5-fold higher permeation after argon plasma irradiation for 60 s. In addition, the time-dependent irradiation of helium plasma also showed an increased absorption ratio of aniline blue dye and finally saturated from the exposure time of 30 s (Figure 4C). When the plasma irradiation distance moved

to 8 mm, there was no significant influence on the absorption rate after irradiation of the argon and helium plasma (Figure 5). Taken together, argon and helium plasma exhibited the most transdermal permeability of aniline blue dye on porcine skin when irradiated for approximately 30 s at a plasma irradiation distance of 4 mm. In addition, argon plasma-treated porcine skin showed higher transdermal permeability than helium plasma. To further investigate the change in temperature by plasma irradiation, we measured the skin temperature after plasma exposure for 10, 30, 60 s at distance of 4 mm. As shown in Figure 6, the skin temperature after exposure of argon plasma for 0, 10, 30, and 60 s was 21.4, 22, 4, 25.9 and 28.7, respectively, and helium plasma was 21.4, 22, 4, 25.9 and 28.7, respectively. The argon and helium plasma treatment for 60 s increased the surface temperature up to approximately 7 °C and 4 °C, respectively.

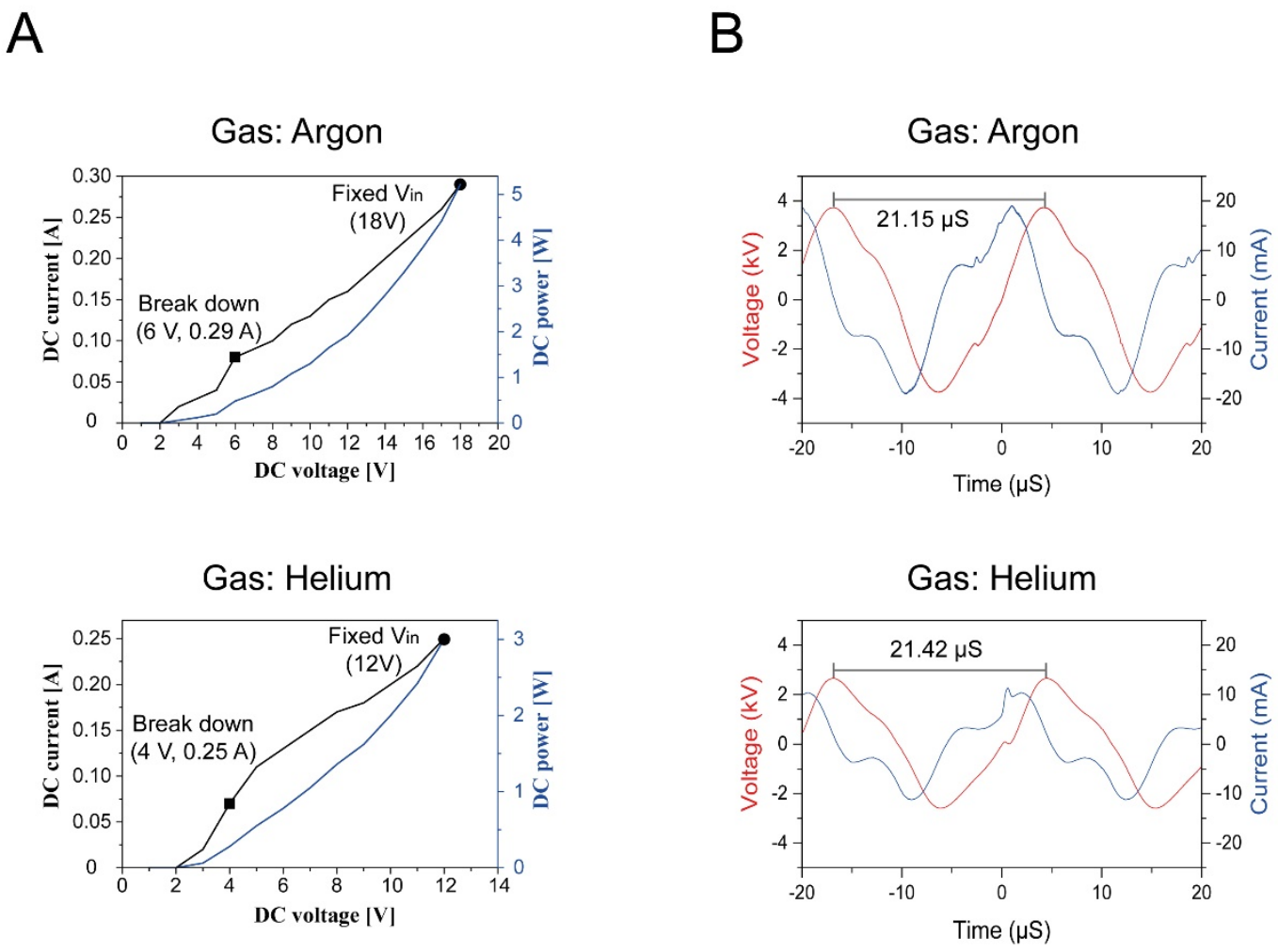

Figure 2. IV curve and electrical waveform of argon and helium plasma jets. The gas flow rates of argon and helium were fixed at 2 slm. (**A**) DC input voltage and DC Discharged current for argon and helium plasma. The breakdown voltage were 6 V for argon and 4 V for helium, The DC input voltage for transdermal permeability experiment were fixed 18 V and 12 V in argon and helium gas, respectively. (**B**) Waveforms of the inverted AC applied voltage and discharge current for the argon and helium plasma at DC input voltage 18 V and 12 V, respectively. The applied RMS voltages were 2.54 kV for argon and 1.73 kV for helium, and their RMS discharge currents were 11.01 mA and 6.21 mA, respectively.

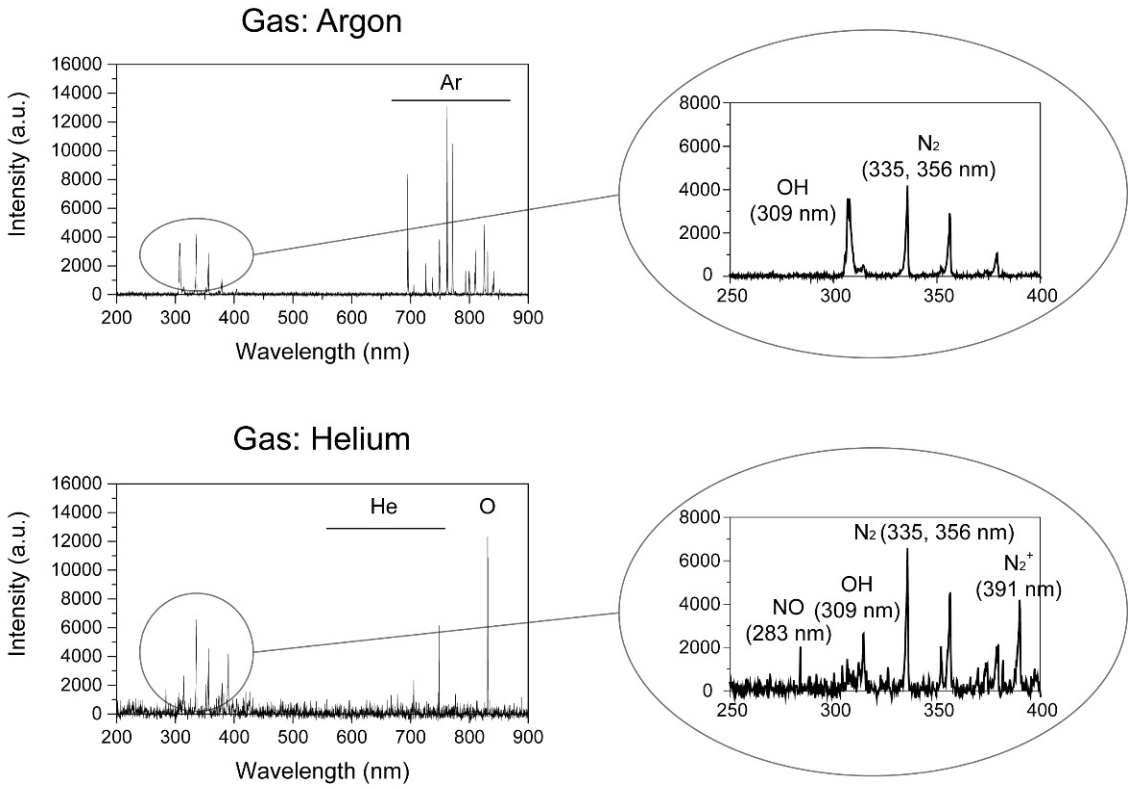

Figure 3. Optical emission spectroscopy of argon and helium plasma jets with a wavelength range from 200–900 nm.

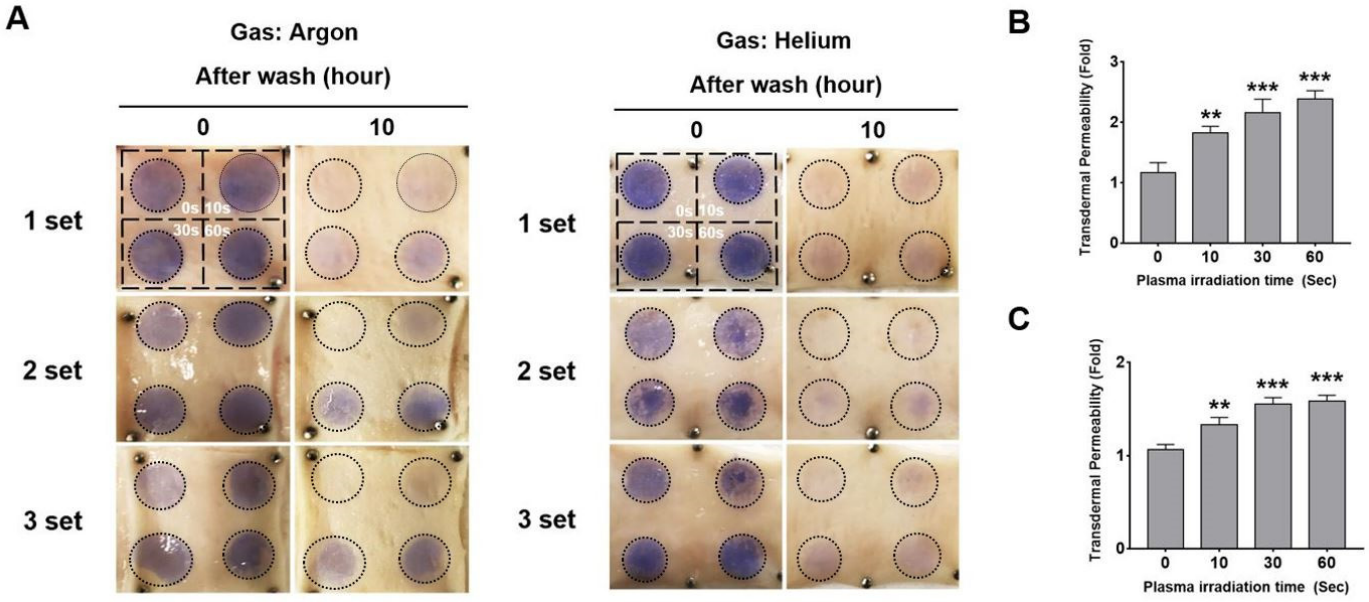

Figure 4. Transdermal absorption of aniline blue dye on porcine skin by argon and helium plasma irradiation at a distance of 4 mm (**A**) The quartered area of the rectangular area in porcine skin was treated with argon or helium plasma for 0, 10, 30, or 60 s at a distance of 4 mm between the plasma jet and the surface of the skin and thereafter stained with aniline blue dye. The transdermal permeability of aniline blue dye on porcine skin was quantified and normalized to that of the nontreated control. (**B**,**C**) Data are presented as means ± S.D. ** $p < 0.01$, *** $p < 0.001$ compared to the nontreated control (one-way ANOVA, Tukey's post hoc test) with argon (**B**) or helium (**C**). n = 3 independent samples per group.

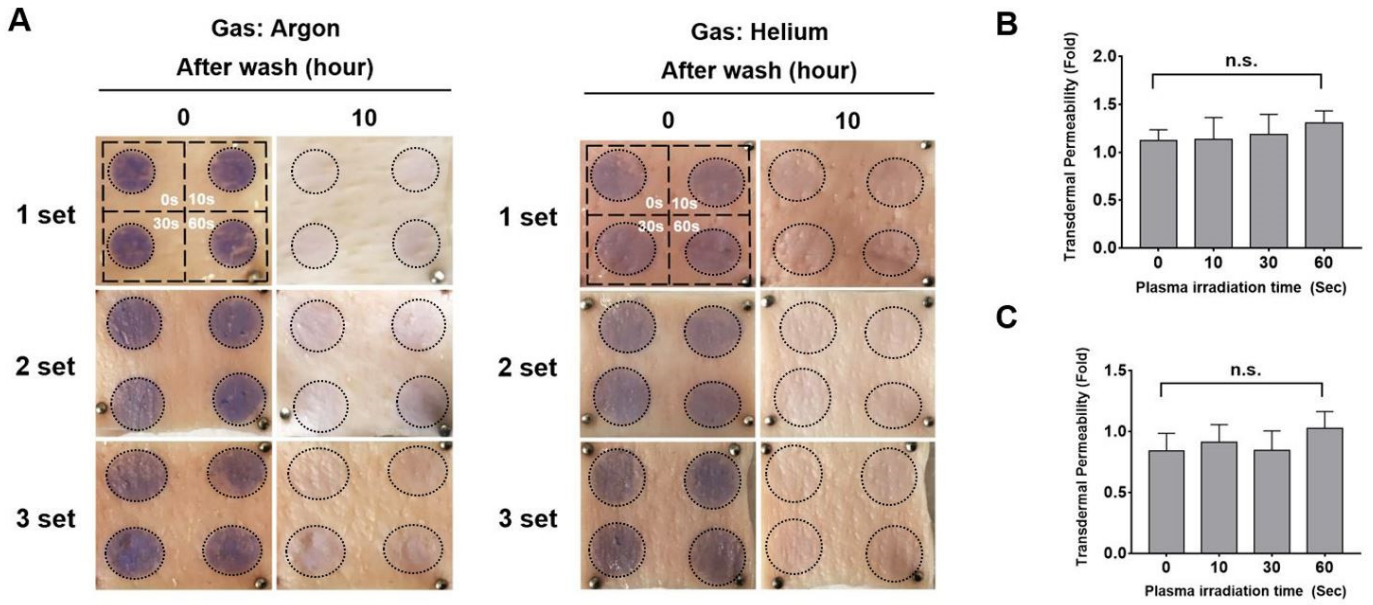

Figure 5. Transdermal absorption of aniline blue dye on porcine skin by argon and helium plasma irradiation at a distance of 8 mm (**A**) The quartered area of the rectangular area in porcine skin was treated with argon or helium plasma for 0, 10, 30, or 60 s at a distance of 8 mm between the plasma jet and the surface of the skin and thereafter stained with aniline blue dye. The transdermal permeability of aniline blue dye on porcine skin was quantified and normalized to that of the nontreated control. (**B**,**C**) Data are presented as means ± S.D. n.s indicates a nonsignificant difference compared to the nontreated control (one-way ANOVA, Tukey's post hoc test) with argon (**B**) or helium (**C**). n = 3 independent samples per group.

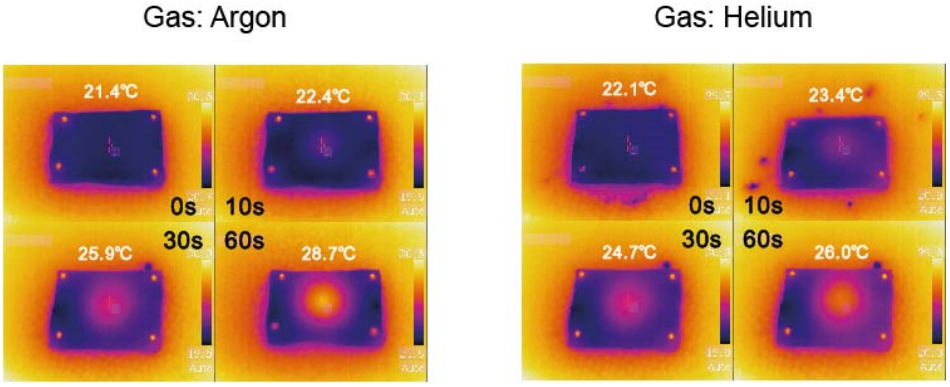

Figure 6. Temperature on porcine skin surface by argon and helium plasma irradiation for 0, 10, 30 or 60 s at a distance of 4 mm between the plasma jet and the surface of the skin.

3.3. Argon Plasma Irradiation Facilitates the Permeability of 70 kDa and 150 kDa Molecules in Keratinocytes

To investigate how to increase transdermal permeability by plasma, we further examined in vitro permeability in keratinocytes that were connected through cell–cell junctions in the epidermal layer. As high-molecular-weight molecules over 1 kDa have difficulty penetrating into the skin, we attempted to compare the penetration of 70 and 150 kDa molecules in keratinocytes with/without argon plasma irradiation. For this purpose, cultured HaCaT cells were first treated with our plasma device for 30 s or not. Subsequently, they were incubated in the medium containing 70 or 150 kDa dextran conjugated with fluorescein for 1 h. Thereafter, the cells were fixed with 4% paraformaldehyde, and the fluorescence intensity inside the cells was observed using a fluorescence microscope. As shown in Figure 7A, fluorescent signals of 70 and 150 kDa dextran were clearly observed in argon plasma-treated keratinocytes, whereas these fluorescent signals were not observed

in nontreated cells. Indeed, statistical analysis revealed that argon plasma irradiation significantly increased the fluorescence intensity of 70 (22.0 ± 4.2) kDa (Figure 7B) and 150 (17.6 ± 3.6) kDa (Figure 7C) dextran in the cells compared to nontreated cells. Therefore, these results suggest that argon plasma irradiation facilitates the penetration of over 1 kDa molecules that generally have difficulty permeating the skin due to their high molecular weight.

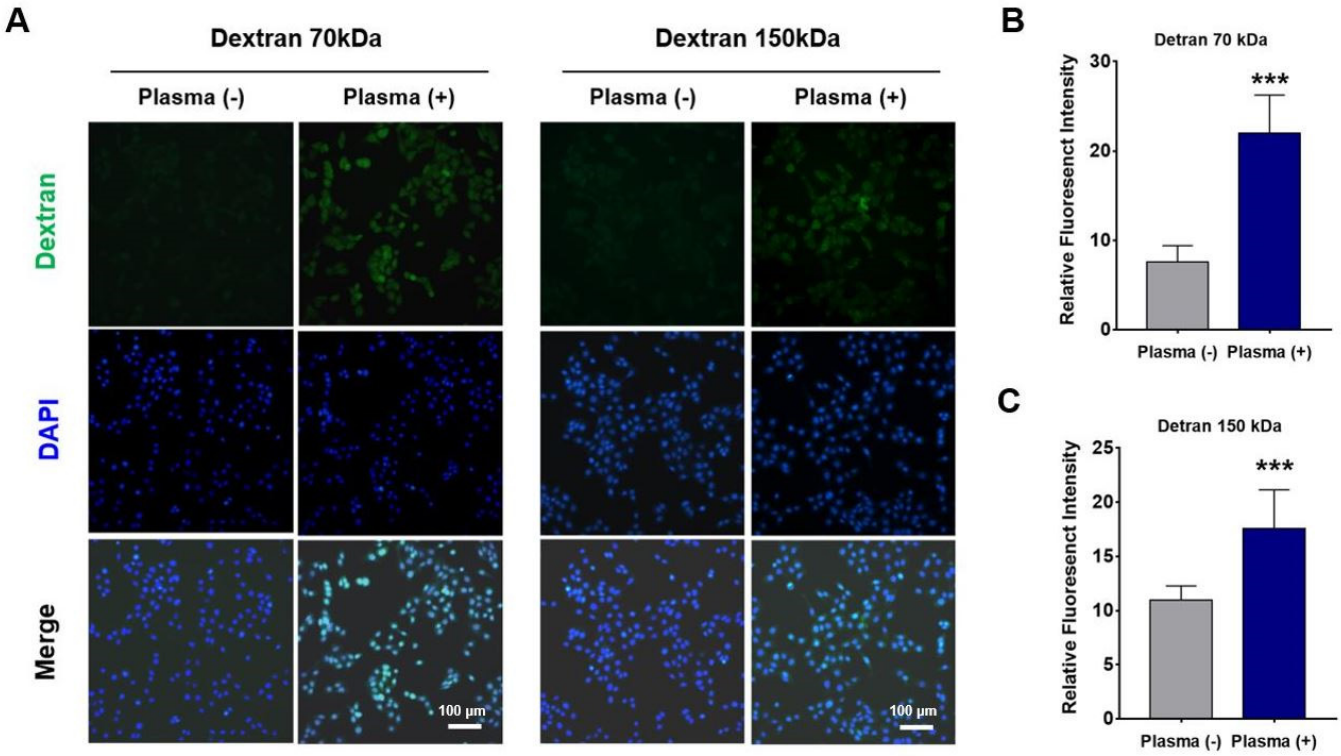

Figure 7. Cellular permeability of 70 kDa and 150 kDa dextran by argon plasma irradiation in keratinocytes. (**A**) Fluorescence images, HaCaT cells were treated with argon plasma for 30 s and then subjected to fluorescein-dextran 70 or 150 kDa. (**B**,**C**) Statistical results of relative fluorescence in the cells treated with 70 kDa (**B**) and 150 kDa (**C**) dextran in the presence and absence of argon plasma irradiation. Scale bar indicates 100 μm. The fluorescent intensity was averaged from 40 cells. Data are presented as means ± S.D. *** $p < 0.001$ compared to the nontreated control (unpaired two-tailed *t*-test).

3.4. Argon Plasma Irradiation Induces the Production of Nitric Oxide in Keratinocytes

Generally, nitric oxide is a free radical with an unpaired electron, and it is well known to regulate various epidermal functions, including epidermal proliferation, differentiation, wound healing, and barrier permeability in the skin [31–33]. In fact, nitric oxide regulates junctional, cytoskeletal, and extracellular matrix proteins. Hence, we believed that nitric oxide was involved in plasma-mediated permeability as a transdermal absorption donor. Therefore, we further investigated whether argon plasma irradiation induces the production of nitric oxide in keratinocytes. Argon plasma was applied to HaCaT cells for 10, 30, and 60 s, followed by incubation for 10, 30, 60, and 120 min. As shown in Figure 8, the exposure of plasma on the cells for 10, 30, and 60 s similarly caused the production of nitric oxide up to approximately 80 μM. Nitric oxide was significantly induced from 60 min after irradiation. These findings suggest that plasma-induced nitric oxides from keratinocytes are able to regulate the junctions between cells and the extracellular matrix in the epidermal layer, which would make the epidermal barrier permeable.

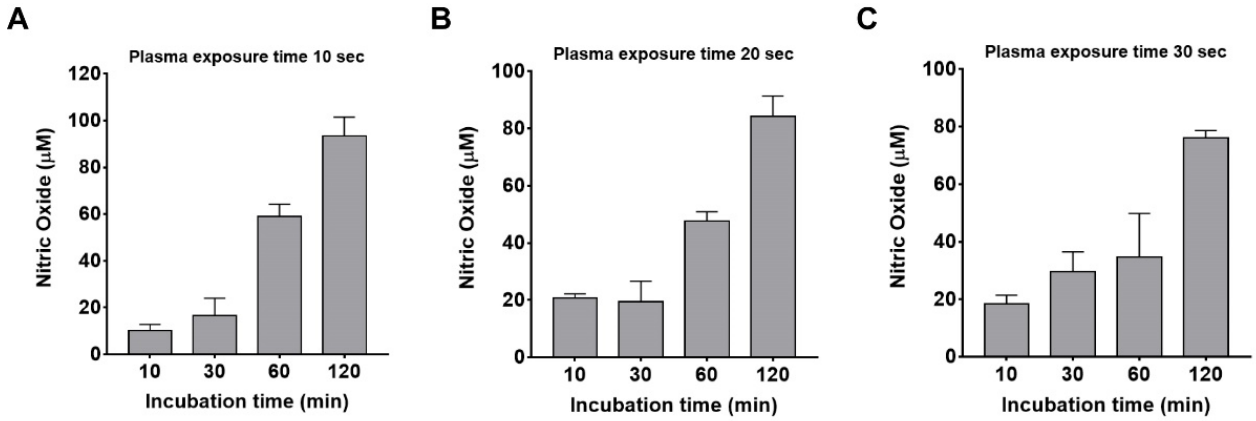

Figure 8. Plasma-induced nitric oxide in the keratinocytes. (**A**–**C**) Argon plasma was applied to keratinocytes for 10 (**A**), 30 (**B**), and 60 (**C**) seconds, followed by incubation for 10, 30, 60, and 120 min. Intracellular nitric oxide levels were measured by quantitative colorimetry at 540 nm from keratinocytes. Data are presented as means ± S.D. n = 3 independent samples per group.

4. Conclusions

The epidermal transmission of nutrients, cosmetics, and drugs is a painless and non-invasive delivery method that has the advantages of providing continuous and long-term release as well as improving patient adaptability. Among current percutaneous transmission methods and technologies, cold plasma can easily irradiate the desired portion of the skin without epidermal damage. Recently, several studies have provided the effect of cold plasma on transdermal permeability. In the present study, an atmospheric-pressure plasma jet device was fabricated to test the transdermal permeability, and its device effectively showed improved permeability of aniline blue dye on porcine skin. Furthermore, we showed a significant increase in the transmission of high-molecular-weight molecules (70 and 150 kDa) with the production of nitric oxide in plasma-treated keratinocytes. Further studies are warranted to clarify the molecular and cellular mechanism(s) underlying plasma-induced nitric oxide and transdermal absorption in keratinocytes.

Author Contributions: Conceptualization, S.L., J.C., Y.J. and T.H.L.; experiments and formal analysis, S.L., J.C. and J.K.; writing and visualization, S.L., J.C., Y.J. and T.H.L. All authors have read and agreed to the published version of the manuscript.

Funding: This research was funded by the MEB research fund of Hanyang University (HY-202000000002924).

Institutional Review Board Statement: Not applicable.

Informed Consent Statement: Not applicable.

Data Availability Statement: The data presented in this study are available on request from the corresponding author.

Conflicts of Interest: The authors declare that they have no conflict of interest.

References

1. Marwah, H.; Garg, T.; Goyal, A.K.; Rath, G. Permeation enhancer strategies in transdermal drug delivery. *Drug Deliv.* **2016**, *23*, 564–578. [CrossRef]
2. Akhtar, N.; Singh, V.; Yusuf, M.; Khan, R.A. Non-invasive drug delivery technology: Development and current status of transdermal drug delivery devices, techniques and biomedical applications. *Biomed. Eng. Biomed. Tech.* **2020**, *65*, 243–272. [CrossRef] [PubMed]
3. Al Hanbali, O.A.; Khan, H.M.S.; Sarfraz, M.; Arafat, M.; Ijaz, S.; Hameed, A. Transdermal patches: Design and current approaches to painless drug delivery. *Acta Pharmaceut.* **2019**, *69*, 197–215. [CrossRef]

4. Waghule, T.; Singhvi, G.; Dubey, S.K.; Pandey, M.M.; Gupta, G.; Singh, M.; Dua, K. Microneedles: A smart approach and increasing potential for transdermal drug delivery system. *Biomed. Pharmacother.* **2019**, *109*, 1249–1258. [CrossRef] [PubMed]
5. Toyoda, M.; Hama, S.; Ikeda, Y.; Nagasaki, Y.; Kogure, K. Anti-cancer vaccination by transdermal delivery of antigen peptide-loaded nanogels via iontophoresis. *Int. J. Pharmaceut.* **2015**, *483*, 110–114. [CrossRef] [PubMed]
6. Cordery, S.F.; Husbands, S.M.; Bailey, C.P.; Guy, R.H.; Delgado-Charro, M.B. Simultaneous Transdermal Delivery of Buprenorphine Hydrochloride and Naltrexone Hydrochloride by Iontophoresis. *Mol. Pharmaceut.* **2019**, *16*, 2808–2816. [CrossRef]
7. Azagury, A.; Khoury, L.; Enden, G.; Kost, J. Ultrasound mediated transdermal drug delivery. *Adv. Drug Deliver. Rev.* **2014**, *72*, 127–143. [CrossRef] [PubMed]
8. Daftardar, S.; Neupane, R.; Boddu, S.H.S.; Renukuntla, J.; Tiwari, A.K. Advances in Ultrasound Mediated Transdermal Drug Delivery. *Curr. Pharm. Des.* **2019**, *25*, 413–423. [CrossRef] [PubMed]
9. Wen, X.; Xin, Y.; Hamblin, M.R.; Jiang, X. Applications of cold atmospheric plasma for transdermal drug delivery: A review. *Drug Deliv. Transl. Res.* **2020**. [CrossRef] [PubMed]
10. Von Woedtke, T.; Schmidt, A.; Bekeschus, S.; Wende, K.; Weltmann, K.D. Plasma Medicine: A Field of Applied Redox Biology. *In Vivo* **2019**, *33*, 1011–1026. [CrossRef]
11. Semmler, M.L.; Bekeschus, S.; Schafer, M.; Bernhardt, T.; Fischer, T.; Witzke, K.; Seebauer, C.; Rebl, H.; Grambow, E.; Vollmar, B.; et al. Molecular Mechanisms of the Efficacy of Cold Atmospheric Pressure Plasma (CAP) in Cancer Treatment. *Cancers* **2020**, *12*, 269. [CrossRef]
12. Hwang, Y.; Jeon, H.; Wang, G.Y.; Kim, H.K.; Kim, J.-H.; Ahn, D.K.; Choi, J.S.; Jang, Y. Design and Medical Effects of a Vaginal Cleaning Device Generating Plasma-Activated Water with Antimicrobial Activity on Bacterial Vaginosis. *Plasma* **2020**, *3*, 204–213. [CrossRef]
13. Cordaro, L.; De Masi, G.; Fassina, A.; Gareri, C.; Pimazzoni, A.; Desideri, D.; Indolfi, C.; Martines, E. The Role of Thermal Effects in Plasma Medical Applications: Biological and Calorimetric Analysis. *Appl. Sci.* **2019**, *9*, 5560. [CrossRef]
14. Bernhardt, T.; Semmler, M.L.; Schafer, M.; Bekeschus, S.; Emmert, S.; Boeckmann, L. Plasma Medicine: Applications of Cold Atmospheric Pressure Plasma in Dermatology. *Oxid. Med. Cell Longev.* **2019**, *2019*, 3873928. [CrossRef] [PubMed]
15. Brany, D.; Dvorska, D.; Halasova, E.; Skovierova, H. Cold Atmospheric Plasma: A Powerful Tool for Modern Medicine. *Int. J. Mol. Sci.* **2020**, *21*, 2932. [CrossRef]
16. Lee, Y.; Ricky, S.; Lim, T.H.; Jang, K.S.; Kim, H.; Song, Y.; Kim, S.Y.; Chung, K.S. Wound Healing Effect of Nonthermal Atmospheric Pressure Plasma Jet on a Rat Burn Wound Model: A Preliminary Study. *J. Burn Care Res.* **2019**, *40*, 923–929. [CrossRef]
17. Boeckmann, L.; Schafer, M.; Bernhardt, T.; Semmler, M.L.; Jung, O.; Ojak, G.; Fischer, T.; Peters, K.; Nebe, B.; Muller-Hilke, B.; et al. Cold Atmospheric Pressure Plasma in Wound Healing and Cancer Treatment. *Appl. Sci.* **2020**, *10*, 6898. [CrossRef]
18. Shimizu, K.; Hayashida, K.; Blajan, M. Novel method to improve transdermal drug delivery by atmospheric microplasma irradiation. *Biointerphases* **2015**, *10*, 029517. [CrossRef] [PubMed]
19. Xin, Y.; Wen, X.; Hamblin, M.R.; Jiang, X. Transdermal delivery of topical lidocaine in a mouse model is enhanced by treatment with cold atmospheric plasma. *J. Cosmet. Dermatol.* **2020**. [CrossRef] [PubMed]
20. Shimizu, K.; Tran, A.N.; Kristof, J.; Blajan, M. Investigation of atmospheric microplasma for improving skin permeability. In Proceedings of the 2016 Electrostatics Joint Conference, West Lafayette, IN, USA, 13–16 June 2016; pp. 13–18.
21. Kristof, J.; Miyamoto, H.; Tran, A.N.; Blajan, M.; Shimizu, K. Feasibility of transdermal delivery of Cyclosporine A using plasma discharges. *Biointerphases* **2017**, *12*, 02B402. [CrossRef] [PubMed]
22. Alkilani, A.Z.; McCrudden, M.T.; Donnelly, R.F. Transdermal Drug Delivery: Innovative Pharmaceutical Developments Based on Disruption of the Barrier Properties of the stratum corneum. *Pharmaceutics* **2015**, *7*, 438–470. [CrossRef]
23. Parhi, R.; Suresh, P.; Patnaik, S. Physical means of stratum corneum barrier manipulation to enhance transdermal drug delivery. *Curr. Drug Deliv.* **2015**, *12*, 122–138. [CrossRef] [PubMed]
24. Marschewski, M.; Hirschberg, J.; Omairi, T.; Hofft, O.; Viol, W.; Emmert, S.; Maus-Friedrichs, W. Electron spectroscopic analysis of the human lipid skin barrier: Cold atmospheric plasma-induced changes in lipid composition. *Exp. Dermatol.* **2012**, *21*, 921–925. [CrossRef] [PubMed]
25. Schmidt, A.; Liebelt, G.; Striesow, J.; Freund, E.; von Woedtke, T.; Wende, K.; Bekeschus, S. The molecular and physiological consequences of cold plasma treatment in murine skin and its barrier function. *Free Radic. Biol Med.* **2020**, *161*, 32–49. [CrossRef] [PubMed]
26. Jang, Y.; Kim, E.K.; Shim, W.S.; Song, K.M.; Kim, S.M. Amniotic fluid exerts a neurotrophic influence on fetal neurodevelopment via the ERK/GSK-3 pathway. *Biol. Res.* **2015**, *48*, 44. [CrossRef] [PubMed]
27. Shao, T.; Zhang, C.; Wang, R.X.; Zhou, Y.X.; Xie, Q.; Fang, Z. Comparison of Atmospheric-Pressure He and Ar Plasma Jets Driven by Microsecond Pulses. *IEEE T. Plasma Sci.* **2015**, *43*, 726–732. [CrossRef]
28. Lee, H.Y.; Choi, J.H.; Hong, J.W.; Kim, G.C.; Lee, H.J. Comparative study of the Ar and He atmospheric pressure plasmas on E-cadherin protein regulation for plasma-mediated transdermal drug delivery. *J. Phys. D Appl. Phys.* **2018**, *51*, 215401. [CrossRef]
29. Bell, K.L.; Dalgarno, A.; Kingston, A.E. Penning Ionization by Metastable Helium Atoms. *J. Phys. Part B Atom. Mol. Phys.* **1968**, *1*, 18. [CrossRef]

30. Liu, Y.; Ni, H.Y.; Wargniez, W.; Gregoire, S.; Durand, I.; Roussel-Berlier, L.; Eilstein, J.; Jie, Q.; Ma, T.; Shen, T.; et al. Inter-laboratory study of the skin distribution of 4-n-butyl resorcinol in ex vivo pig and human skin. *J. Chromatogr. B* **2018**, *1093*, 77–79. [CrossRef] [PubMed]
31. Dang, E.L.; Man, G.; Zhang, J.C.; Lee, D.; Mauro, T.M.; Elias, P.M.; Man, M.Q. Inducible nitric oxide synthase is required for epidermal permeability barrier homeostasis in mice. *Exp. Dermatol.* **2020**, *29*, 1027–1032. [CrossRef] [PubMed]
32. Vaccaro, M.; Irrera, N.; Cutroneo, G.; Rizzo, G.; Vaccaro, F.; Anastasi, G.P.; Borgia, F.; Cannavo, S.P.; Altavilla, D.; Squadrito, F. Differential Expression of Nitric Oxide Synthase Isoforms nNOS and iNOS in Patients with Non-Segmental Generalized Vitiligo. *Int. J. Mol. Sci.* **2017**, *18*, 2533. [CrossRef] [PubMed]
33. Ikeyama, K.; Denda, M. Effect of endothelial nitric oxide synthase on epidermal permeability barrier recovery after disruption. *Br. J. Dermatol.* **2010**, *163*, 915–919. [CrossRef] [PubMed]